Estimation of Jiles–Atherton Parameters of Toroid Cores Using MATLAB/Simulink

Š. Gans*, J. Molnár and D. Kováč

Department of Theoretical and Industrial Engineering, Faculty of Electrical Engineering and Informatics, Technical University of Košice, Park Komenského 3, 040 01 Košice, Slovak Republic

Received: 28.10.2022 & Accepted: 17.03.2023

Doi: 10.12693/APhysPolA.143.389 *e-mail: simon.gans@tuke.sk

This paper addresses the development and testing of a new genetic-like algorithm for the Jiles–Atherton ferromagnetic hysteresis model parameter fitting. The MATLAB/Simulink environment was used for the simulation and postprocessing of data. Firstly, the model's first-order ordinary differential equation is introduced with a brief description of its parameters. A correction parameter was introduced into the equation to eliminate the non-physical behavior of the model. Then the fitting algorithm and fit function are described. An experimental setup is built to measure the hysteretic loops of a ferromagnetic toroid core consisting of an iron powder material. The major and several minor hysteresis loops were measured and used as inputs into the model fitting algorithm. The measurement is then compared with the simulated results.

topics: BH curve, hysteresis, Jiles–Atherton, MATLAB

1. Introduction

Several problems arise when designing electrical machines like transformers and motors. One such problem is the development of a reliable hysteresis model of ferromagnetic materials. Such descriptions can find use in the studies of hysteresis loss, which manifests itself in heat dissipation during the remagnetization of ferromagnetic and ferrimagnetic materials. The heating effect arises from the fact that on a microscopic scale, a part of the magnetization process is due to domain wall movements. The domain walls attach to and detach from pinning sites according to the local magnetic field acting on them. Wall jumps create a change in magnetic flux and thus generate eddy currents that dissipate energy due to the Joule effect. Since temperature is a factor strongly affecting ferromagnetic material properties (study [1] showed the temperature effect on magnetization curves for special materials), describing the losses accurately is crucial [2, 3].

Multiple ways of hysteresis modeling have been studied in the past. The Preisach model [4] is a common method used for this task, but it needs a lot of measurement data for its parameters to be determined, and they have a statistical non-physical nature. The material is thought to consist of a distribution of elementary hysteresis relay-type operators, which switch their outputs between +1 and −1. The probability density function of the hysteresis operator's switching states must be fitted from experimental data, and it is a material characteristic that defines the shape of the major loop and any trajectory inside it (minor loops) [4]. The combination of Jiles–Atherton (J-A) and Preisach models with the theory of Néel's fluctuating field introduced an exponential model [5], which was able to accurately predict even more intricate magnetic behaviors, but is rather complex. The Harrison model was also implemented for specific material types [6]. A substantial difference between the J-A model and the Harrison model is that the reversible and irreversible magnetization equations are decoupled in the Harrison model, whereas in the J-A model, they are coupled by an effective field variable. Also, in the Harrison model, domain pinning is not the primary source of hysteresis — rather, it is assumed that it has mainly a quantum origin. Both models require parameters as inputs, but in the case of the Harrison model, the parameter values are based on the physical aspects of the sample and the environment so they can be evaluated directly, although some parameters are dependent on one or more variables and are usually for simplicity's sake taken to be constant, which still yields good results for the description of static loops at specific excitations. Both models make use of the Langevin function, but in a different way, which is described in more detail in [7].

TABLE I
Jiles–Atherton model parameters.

Parameter	Physical units
M_s	[A/m]
α	[1]
k	[A/m]
c	[1]
a	[A/m]

Study [8] also showed the temperature dependence of J-A model parameters in reference to magnetocaloric compounds. Energy-based models were proposed [9] that have multiple parameters and are based on a set of simplifying assumptions to make the model computable. However, the most used model today for modeling hysteresis is the Jiles–Atherton model, originally developed in 1984 [10]. It stands out due to its simplicity and the physical nature of its parameters. It is modeled by one ordinary differential equation. The cost of using the J-A model is that some minor loops tend to be modeled less accurately because the parameters exhibit a dependence on the field strength and therefore are not constant for various minor loops [11], which is solved by using field-dependent c and k parameters. Some studies pointed out the intricacies of the model that lead to non-physical behavior [12]. The non-physicality stems that in the model, several terms that the model is defined upon are unphysical, e.g, defining work done in terms of co-energies. The anhysteretic curve shown in [12] has its trajectory passing through the second quadrant of the M–H plane, which is not consistent with experiments. This sets the anhysteretic curve that the J-A model heavily relies upon, as a skeleton of the model upon which the hysteresis loop is built, and not much more. The respective authors of the study [12] suggest that due to these observations, the J-A model should be used as a tool in electrical simulators and spice models to define hysteresis loop shapes.

Several alterations of the original static J-A model have been developed such as the dynamic frequency-dependent J-A model [13] and a mechanical stress-dependent model [14]. The simplicity of the J-A model enabled it to be easily implemented into finite element method (FEM) simulation algorithms [15]. The ongoing research suggests that its popularity will not end anytime soon. A more detailed comparison between the most frequently used models can be found in [16]. Symmetrical hysteresis loops can also be modeled via the hyperbolic tangent functions [17].

The most challenging aspect of employing the J-A model is fitting its parameters to experimental data. The model is extremely sensitive to initial parameter values used for the optimization problem to minimize the sum of squared errors (SSEs) that quantifies the difference between the simulated and measured hysteresis loops. The SSE exhibits multiple local minima in the parameter space [18]. Researchers successfully employed many different methods to approach this problem, such as space-filling designs and genetic algorithms [18], particle swarm optimization [19], simulated annealing method [20], numerical iterative algorithms like the Levenberg–Marquardt algorithm [21], deterministic sampling algorithms like the DIRECT algorithm [22], random and deterministic searches [23], and more. In this paper, a random search algorithm is developed and tested.

2. The Jiles–Atherton hysteresis model

The J-A model describes the nonlinear nature of magnetic materials by defining the shape of their BH curve. The theoretic background is based on the Weiss molecular field theory, the theories of Langevin, and the assumption that domain walls are elastic and can bend to a certain degree while being pinned to a pinning site [10, 24].

In ferromagnetic materials, because there exists a coupling between domains when magnetized, this effectively changes the magnetic field acting on them. Therefore, an effective field is defined as

$$H_e = H + \alpha M, \tag{1}$$

where H_e is the effective magnetic field, and α is the mean-field coupling parameter, whose value will be determined by the fitting process [10].

First, anhysteretic magnetization is defined, which describes the dependence of the magnetization on the effective field of an ideal ferromagnetic material in its global equilibrium state with no defects or pinning sites. The anhysteretic magnetization can be measured experimentally for a non-ideal material [25], but it is considered challenging to do accurately. The anhysteretic magnetization M_{an} is commonly defined by the Langevin function as

$$M_{\mathrm{an}}(H_e) = M_S \left[\coth\left(\frac{H_e}{a}\right) - \frac{a}{H_e} \right], \tag{2}$$

where a is a parameter that adjusts the shape of the anhysteretic magnetization function, and M_S is the magnetization at technical saturation, which is the maximum amount of magnetization the material can attain when exposed to large magnetic field strengths. The Langevin function was chosen arbitrarily. Other functions were employed as well in different studies, like the hyperbolic tangent function and the double Langevin function [26], which fit the experimental data well for specific materials [10].

In a real hysteretic material, the magnetization cannot reach its equilibrium state, and the difference between the magnetization and the anhysteretic magnetization determines the bending of domain walls, which tries to reduce this difference [10].

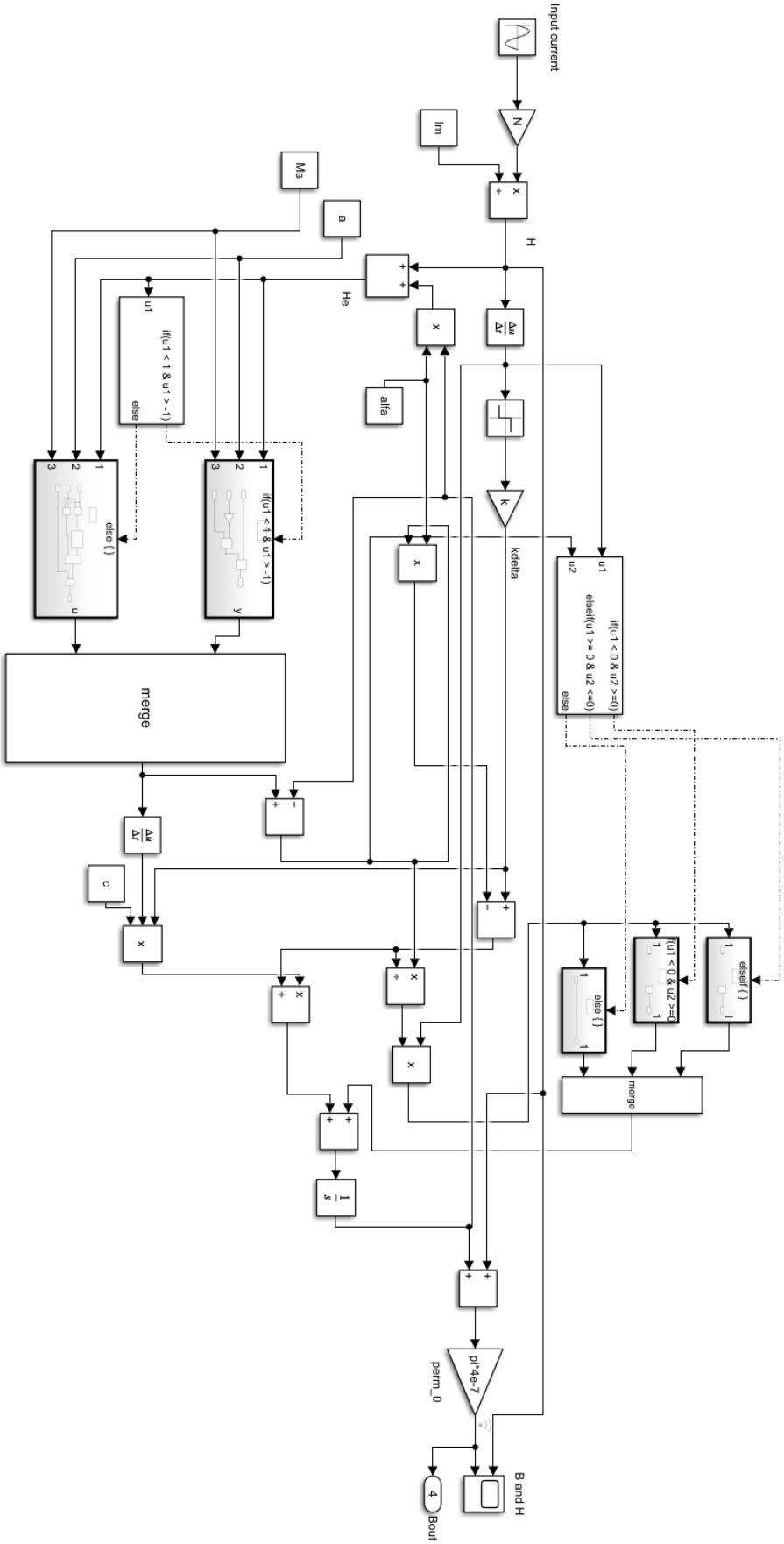

Fig. 1. The developed Simulink model that implements the differential equation of the J-A model.

There exist several different versions of the J-A model. A detailed discussion can be found in the recently published paper [27]. To create the model used in this study, we have chosen the following expression for the differential susceptibility

$$\frac{\mathrm{d}M}{\mathrm{d}H} = \frac{M_{\mathrm{an}} - M}{k\delta - \alpha\left(M_{\mathrm{an}} - M\right)} + \frac{ck\delta}{k\delta - \alpha\left(M_{\mathrm{an}} - M\right)} \frac{\mathrm{d}M_{\mathrm{an}}}{\mathrm{d}H}, \tag{3}$$

which can be found in the paper by Jiles and Atherton from 1986 [10]. In this expression, there are two terms: the first one is related to the irreversible magnetization process, and the second one is to the reversible process, which is due to domain wall bowing. The reversible process is weighted by the c coefficient. Model parameter k is expressed in A/m, as suggested in the 1992 paper by Jiles, Thoelke, and Devine [28]. This parameter is related in magnitude to the coercive field strength, according to the mentioned authors. It is worth noting that δ determines the sign of the field strength derivative and is introduced to distinguish between the ascending and descending loop branches.

3. MATLAB/Simulink model

The input into the model is the magnetizing current of the primary coil wound on a toroid core, which is the subject of analysis, and the output of the model is the magnetic flux density B inside the core. The magnetic field intensity in the core is approximated by

$$H = \frac{NI}{l_e}, \tag{4}$$

where N is the number of turns of the primary coil and l_e is the average magnetic field line length in the core. Because the Simulink software only allows us to do time derivation and integration, we express the model by

$$M(t) + M_0 = \int \mathrm{d}t \, \frac{(M_{\mathrm{an}} - M)}{k\delta - \alpha\left(M_{\mathrm{an}} - M\right)} \frac{\mathrm{d}H}{\mathrm{d}t} + \int \mathrm{d}t \, \frac{ck\delta}{k\delta - \alpha\left(M_{\mathrm{an}} - M\right)} \frac{\mathrm{d}M_{\mathrm{an}}}{\mathrm{d}t}. \tag{5}$$

A similar modeling approach was taken in the study [29], where the authors implemented a Jiles–Atherton model with a heuristic fitting process. Using the Simulink model in the current state of development of the software has been made easy by special Simulink tools, such as the parameter estimator application, which comes with various fitting algorithms to fit experimental data.

Note that (5) can be directly modeled in MATLAB/Simulink. The value of M_0 (the initial condition of the integrator) should be set from the first data point of the measured B and H waveforms. One problem of the model is that when the effective field H_e is close to 0, the anhysteretic magnetization function (2) approaches singularities. One way of solving this is to use the Taylor expansion of the function, i.e.,

$$M_{\mathrm{an}} = \begin{cases} \frac{1}{3} M_S \frac{H_e}{a}, & \text{if} \quad |H_e| < 0.5, \\ M_S \left[\coth\left(\frac{H_e}{a}\right) - \frac{a}{H_e}\right], & \text{if} \quad |H_e| \geq 0.5, \end{cases} \tag{6}$$

when H_e is smaller than an arbitrary small number that avoids these singularities. In the model, this limit is set to a field intensity of 0.5 A/m [15].

However, (5) still shows non-physical behavior most prominently near the tips of the hysteresis loops, where negative differential permeability can be observed. This can be fixed by introducing a parameter δ_m [12], defined as

$$\delta_m = \begin{cases} 0 \text{ if } \frac{\mathrm{d}H}{\mathrm{d}t} < 0 \text{ and } M_{\mathrm{an}} - M > 0, \\ 0 \text{ if } \frac{\mathrm{d}H}{\mathrm{d}t} > 0 \text{ and } M_{\mathrm{an}} - M < 0. \\ 1 \text{ otherwise} \end{cases} \tag{7}$$

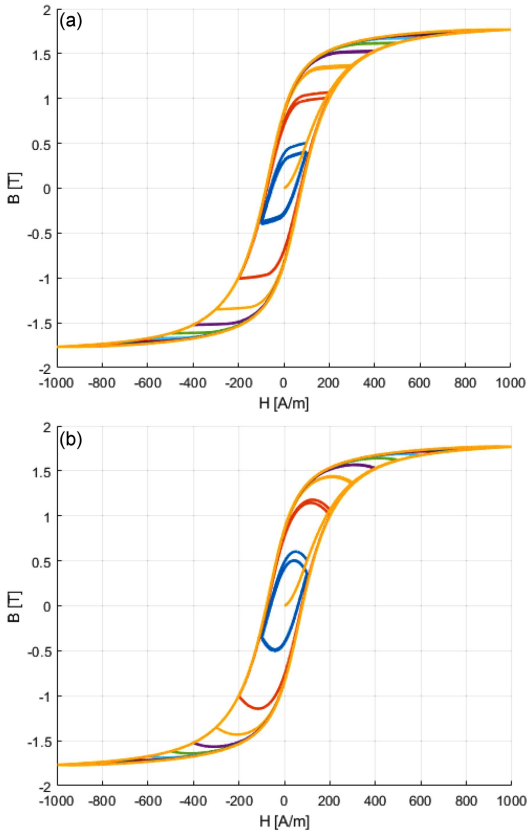

Fig. 2. The difference created between the simulated minor and major hysteresis loops (BH curves (a) with δ_m and (b) without δ_m) when using the introduced delta parameter. Both curves were created using the same model parameters. Nonphysical behavior can be observed, especially in the case of minor loops; $M_s = 1.5 \times 10^6$ A/m, $a = 60$, $c = 0.1$, $\alpha = 4.437 \times 10^{-5}$, $k = 100$ A/m.

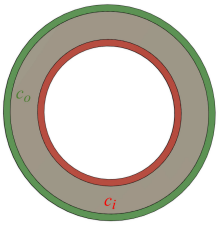

Fig. 3. The model of the measured toroid core. The average magnetic field length inside the core was taken as the average of c_0 and c_i (l_m = 60.947 mm).

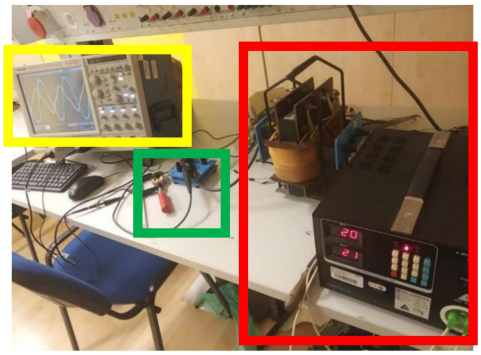

Fig. 4. The practical realization of the measurement setup.

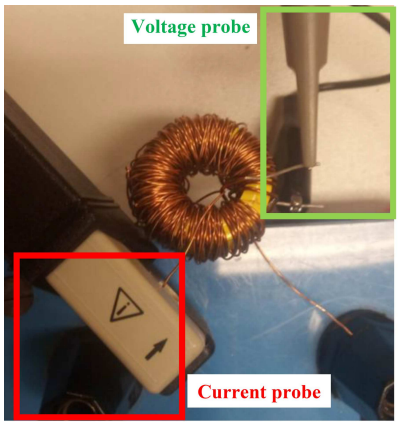

Fig. 5. A toroid-shaped yellow iron powder core was measured. The resulting BH curves can be seen in Fig. 6.

The parameter is then inserted into (5) [12], which becomes

$$M(t) + M_0 = \int \mathrm{d}t \, \frac{\delta_m (M_{\mathrm{an}} - M)}{k\delta - \alpha (M_{\mathrm{an}} - M)} \frac{\mathrm{d}H}{\mathrm{d}t}$$

$$+ \int \mathrm{d}t \, \frac{ck\delta}{k\delta - \alpha (M_{\mathrm{an}} - M)} \frac{\mathrm{d}M_{\mathrm{an}}}{\mathrm{d}t}. \tag{8}$$

The developed Simulink model is shown in (Fig. 1).

The difference which the new parameter δ_M makes can be seen in Fig. 2. The number of turns of the coil N was set to 500, and the magnetizing

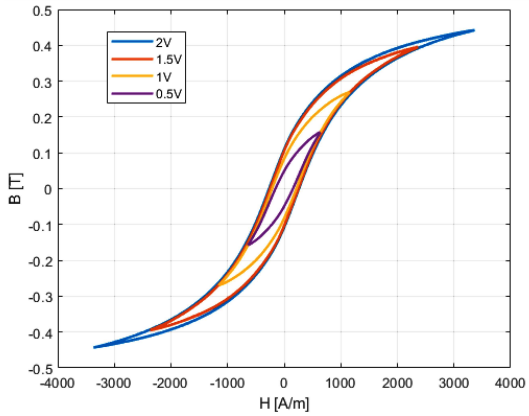

Fig. 6. The measured BH curves of the materials at different saturation levels.

current was defined as having a sinusoidal waveform with an amplitude of 1 A and a frequency of 50 Hz. The equivalent magnetic circuit length l_m was chosen to be the average of the inner ($c_i \approx$ 46.496 mm) and outer ($c_o \approx$ 75.398 mm) circumference of the toroid core (Fig. 3).

The J-A model is quasi-static and therefore frequency independent. For the simulation of the static loops, we used a sinusoidal 50 Hz H waveform, and the simulation time was set to be from time $t = 0$ to t = 40 ms, which captures two periods of the 50 Hz input current signal. The step size was set to be automatically determined by the solver, which used the build-in ode45 solver, based on an explicit Runge–Kutta (4,5) formula, the Dormand–Prince pair. The computation time of a single simulation run was shorter than 1 s.

4. Measurement of hysteresis curves

The measurement setup is shown in Fig. 4. The red rectangle depicts the energy source, which is a laboratory sinusoidal voltage source with a controllable output RMS voltage from 0 to 250 V with a 1 V resolution. Study [30] showed that the frequency at which the hysteresis loop can be considered static is around 1 Hz for specific materials, but naturally, even lower frequencies are preferred. It is connected to a step-down transformer with a transformation ratio of 10:1 to make the supply voltage resolution at the output of the transformer approximately 100 mV. The sinusoidal voltage creates the magnetizing current. The input current of the magnetizing coil of the sample is measured with Hall probes. The induced voltage of the secondary coil is also measured on a different channel. The voltage is then numerically integrated to obtain the B values in the sample (Fig. 5), i.e.,

$$B(t) = -\frac{1}{N_2 S_e} \int_0^t \mathrm{d}t \; u_2(t) + B_0, \tag{9}$$

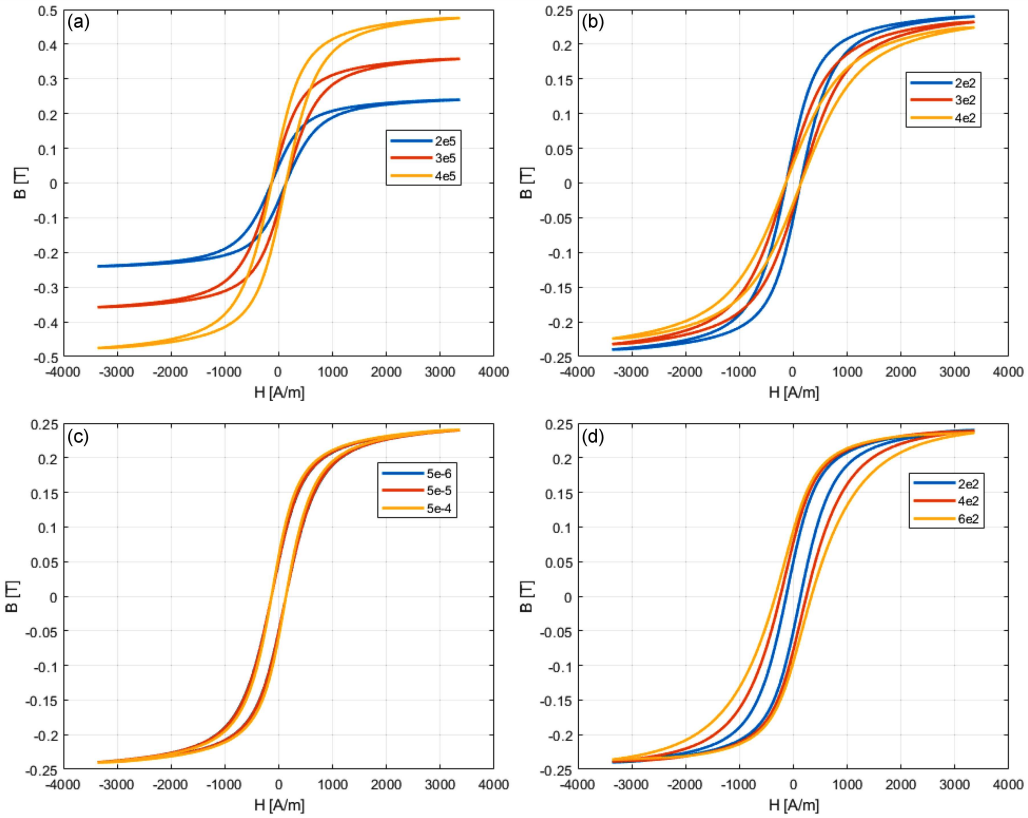

Fig. 7. Variation of a single parameter ((a) M_s, (b) a, (c) α, (d) k) of the model and the shape changes it produces.

where $u_2(t)$ is the secondary coil voltage, N_2 is the number of turns of the secondary coil, and S_e is the effective magnetic circuit cross-section [12].

The magnetic field intensity in the core is computed by using (4). For a detailed description of the measurement setup, the authors redirect the reader to [31]. The material used for this measurement is a carbonyl iron powder mix core that was used in a 3 A 100 μH toroidal inductor. The number of primary and secondary coil turns was 120 and 80, respectively. Copper wire with a diameter of 0.3 mm was used for the windings.

The waveforms were measured by a Tektronix digital storage oscilloscope (DSO) visible in the yellow rectangle in Fig. 4, and the measured sample is shown in the green rectangle (also Fig. 4) and in more detail in Fig. 5.

After measuring multiple periods of voltage and current signals, the signal was post-processed to filter out the noise by using moving mean functions and other commonly employed techniques. The final BH curves can be seen in Fig. 6.

The measurement of hysteresis curves was done on a Tektronix DPO7354 4-channel oscilloscope. The H values were determined from the primary current measured by a hall probe, whose maximum error in the datasheet is given as 1%. The maximum current during the measurement was 4.67 A, and it was measured on the 5 A range of the probe. The analog channels, when the 200 mV per division is used, have a maximal DC gain error of 2%. In addition, a component of 1.4% of the full-scale rating of the oscilloscope must be considered (the full-scale is understood as the software zoom of the oscilloscope, or 1.2 V when using the 200 mV per division setting). When measuring the largest loop, the maximum induced voltage in the secondary coil was 1.068 V. When measuring the dimensions of the sample, we used mechanical calipers with an accuracy rating of 0.1 mm. Using the expressions from the study [32] to compute the uncertainty of the measured BH loops, we get an uncertainty value of 0.01106 (i.e., $\approx$ 1.1%) for the H measurement. The uncertainty of the induced voltage measurement was 2.85% when using the specifications given by the oscilloscope's user manual. The variance of the integrator was assumed to be like the one computed in the mentioned study [31] (but the computation of the error was simplified due to the complexity of the problem) and therefore was assumed to be 0.0000082. The sample cross-section is rectangular with dimensions of 10 and 5 mm. The same calipers as above were used for this measurement, and uncertainty of the cross-section measurement of 0.0086602 was obtained (i.e., $\approx$ 0.866%). When combining these three uncertainties into one, we get a combined uncertainty of 0.0297867, i.e., $\approx$ 2.9786% for the

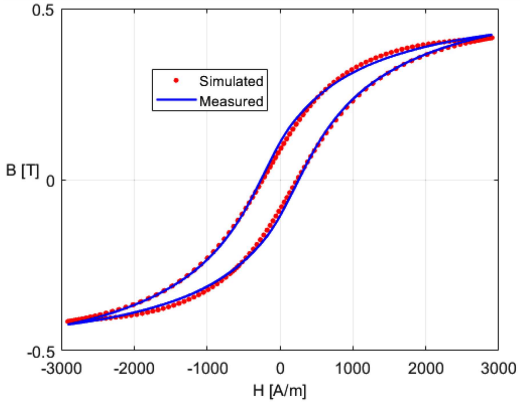

Fig. 8. Comparison of the measured and simulated BH minor curves with optimized parameter values ($M_s = 405151$, $a = 542$, $c = 0.531$, $\alpha = 0.001$, $k = 579$). The measured curve presents the "2 V" curve in Fig. 6.

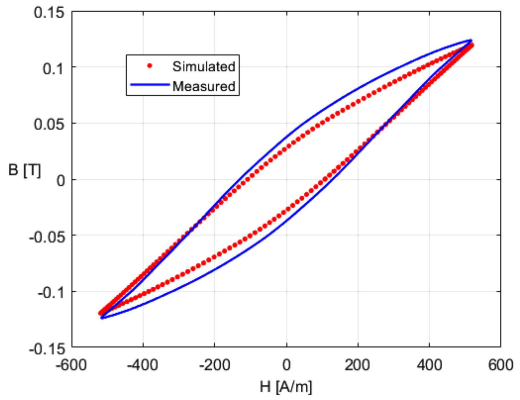

Fig. 9. Comparison of the measured and simulated BH minor curves with the same values as in Fig. 8 but using the same excitation as for the "0.5 V" curve in Fig. 6. It is therefore evident that (at least some) J-A model parameters are excitation dependent.

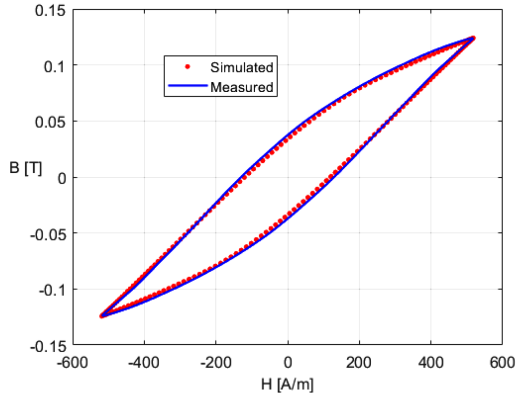

Fig. 10. Comparison of the measured and simulated BH minor curves with optimized parameter values ($M_s = 475368$, $a = 697$, $c = 0.494$, $\alpha = 8.969 \times 10^{-4}$, $k = 327$). The measured curve presents the "0.5 V" curve in Fig. 6.

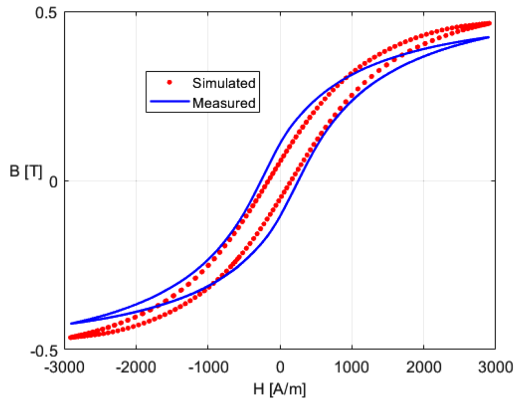

Fig. 11. Comparison of the measured and simulated BH major curves with the same values as in Fig. 10 but using the same excitation as for the "2 V" curve in Fig. 6. The fitted parameters for different minor loops do not characterize all minor loops, which is typical for the J-A model.

B measurement, which is a lot larger compared with the respective authors' study, where they used a REMACOMP® C-200 measuring system, which also was certified, and the uncertainties were quantified by the manufacturer. In our case, only the maximum errors guaranteed by the manufacturers were used, so the final uncertainties may be well over-estimated.

5. Fitting process

To estimate the J-A model parameters for the given hysteresis loops, a parameter estimating algorithm was developed. Study [24] showed that every parameter has an influence on the shape of the hysteresis loop, and this is also shown in Fig. 7. From Figs. 8–11 it is evident that the parameter values depend on the excitation.

Some papers aid the estimation process with analytical approaches that limit the search space [33]. In this work, we employed an estimation method by random search. After some experimentation with different methods, like the pattern search using the Latin hypercube method [34] and the trust-region reflective nonlinear least square algorithm method [35], they optimized the values to some extent, but we tried to implement our estimation algorithm, which is defined by the flowchart in Fig. 12.

How well the applied model parameters fit experimental data was quantified by employing the sum of squares error (SSE), which is computed for every simulation output and is defined by

$$\text{fit} = \frac{1}{N}\sqrt{\sum_{i=1}^{N}\left(\frac{B_{\text{exp}}(i) - B_{\text{sim}}(i)}{\max\left(B_{\text{exp}}\right)}\right)^2}, \qquad (10)$$

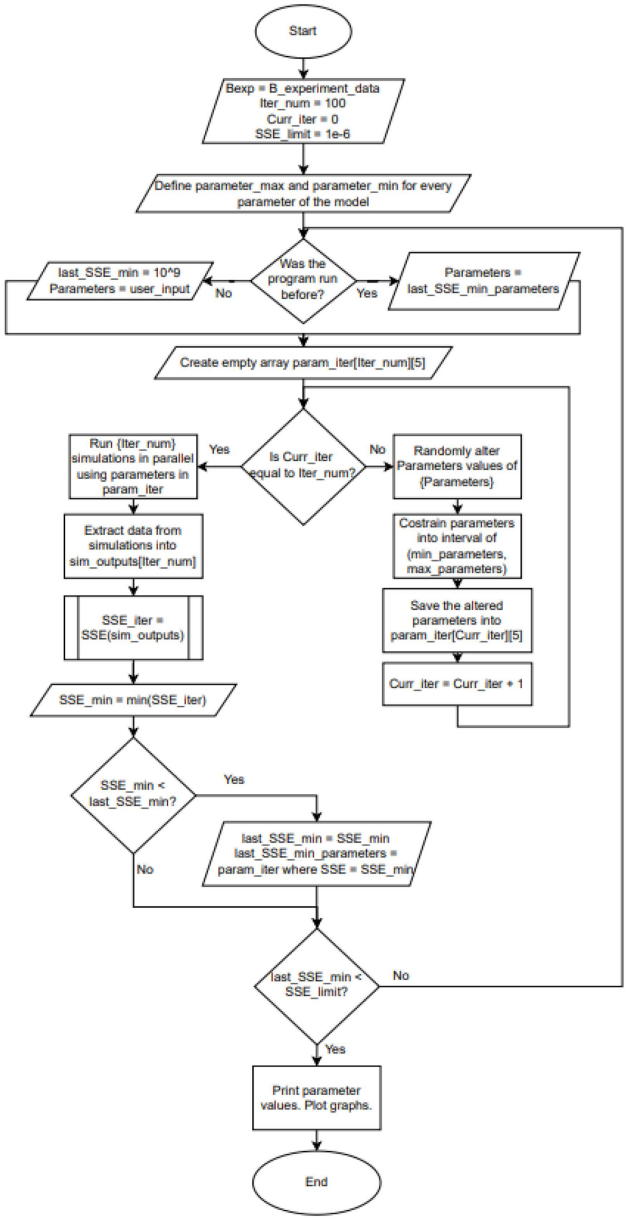

Fig. 12. Flowchart of the developed parameter estimation algorithm.

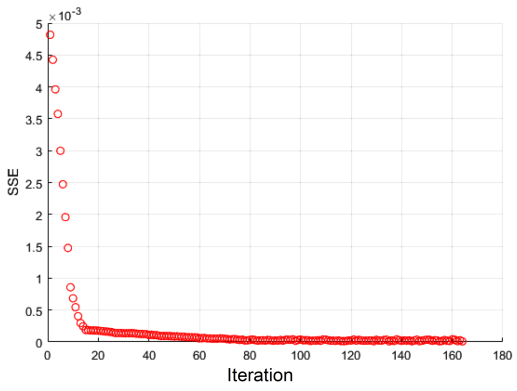

Fig. 13. The time evolution of the fitting process in 165 iterations. The minimum SSE value reached was 9.7336×10^{-6}.

where N is the number of experimental data points, $B_{\mathrm{exp}}(i)$ is the i-th data point of the magnetic flux measurement, and $B_{\mathrm{sim}}(i)$ is the i-th data point of the magnetic flux estimation in the core. The optimization should therefore minimize the fit score by iteratively changing the parameters in a specific way using predefined rules [19].

To further aid the fitting process, parameter bounds were set as described in the study [36]. Setting borders of the search space prevents the algorithm from searching through unreasonable parameter values.

To shorten computation times, the simulation output time was truncated only to simulate through to the upper tip of the hysteresis curve peak, not full loops. The simulation time was shortened from a time interval of 43 to 6 ms. The time evolution of

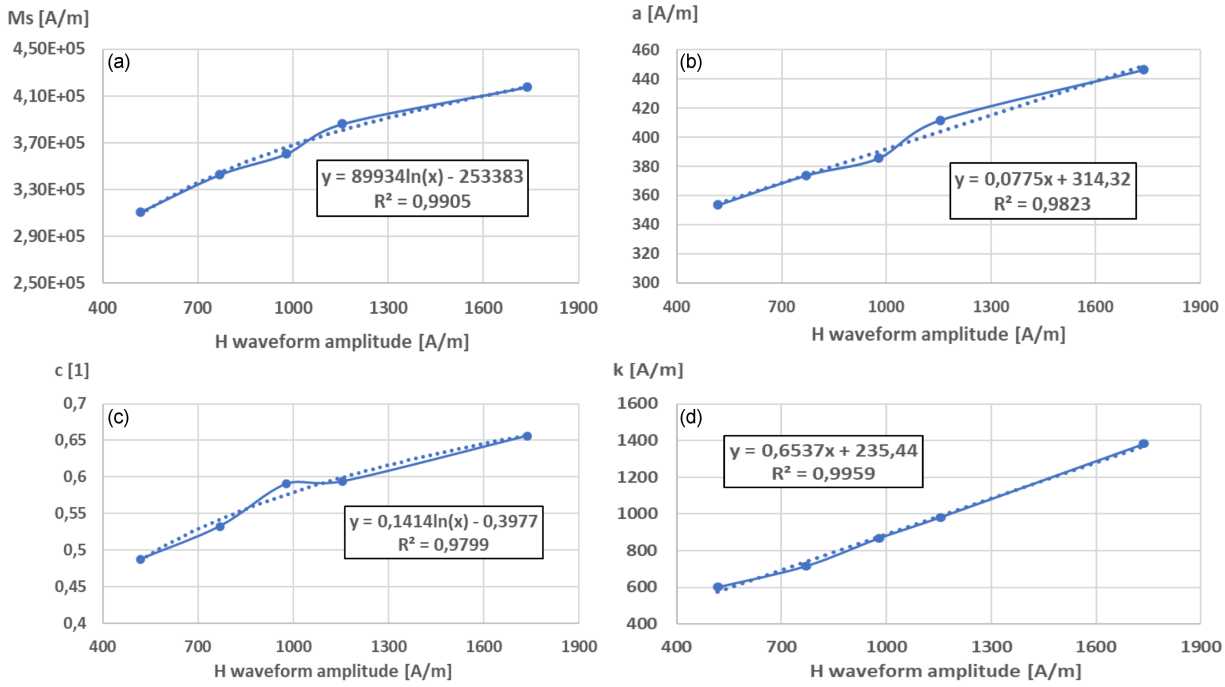

Fig. 14. Graphs of Jiles–Atherton model parameters dependence on the excitation field amplitude. The M_s (a) and c (c) parameters were fitted using a logarithmic fit, and the a (b) and k (d) parameters were fitted with a linear fit. This combination yielded the best simulation results for other excitation waveforms.

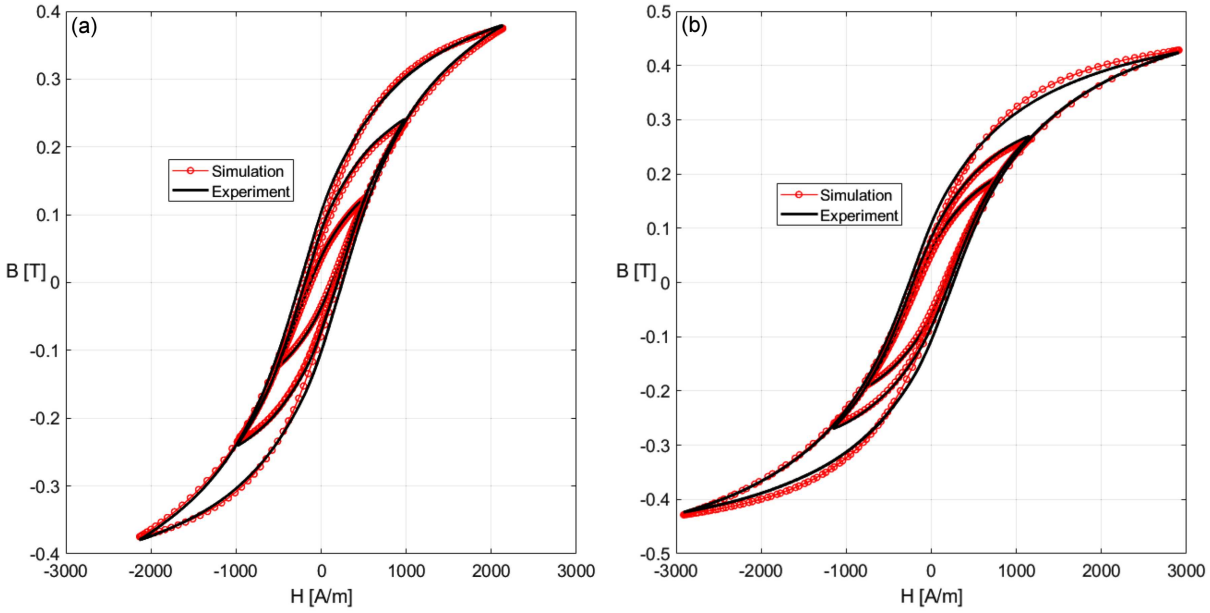

Fig. 15. Example curves (a), (b) fit by using the parameter fit expression formulas. The formulas fit best for lower excitation formulas.

the SSE value throughout the iterations can be seen in Fig. 13. A minimum SSE value of 9.7336×10^{-6} was reached after 165 iterations. The number of simulations evaluated was 16500, and by using parallel computing on 4 Intel i5-8300H processor cores, the total optimization time was approximately 30 min. The graphical comparison of the measured and simulated BH curves can be seen in Figs. 8–11.

6. Excitation dependence of Jiles–Atherton model parameters

Because of this phenomenon, an excitation dependence formula was sought to estimate the Jiles–Atherton model parameters for a given excitation. More specifically, a dependence of the excitation H-field amplitude was taken as the independent

variable. Multiple approaches were considered, and many simulations were done with different excitation waveforms. What was found is that the parameters for this specific material are experiencing linear and logarithmic excitation dependence that could be fitted with an R^2 value larger than 0.98. A dataset of 5 parameter sets was fitted from 5 different excitation values, and a least square method was employed to find the best fit for the given data. To test the expressions, other excitation values were used for the models, and parameter values were computed by them. After experimenting with some sets of fitted parameter values, a promising approach was to set the α parameter constant at a value of $\alpha = 10^{-3}$ and let the other parameters vary by the fitting process. Then, when further analyzing the 5 different excitation waveform amplitude curves, we obtained the graphs shown in Fig. 14.

The found expressions for parameter values were used for the given and other excitations waveforms, and the results shown in Fig. 15 were obtained. A MATLAB script was written to analyze the H waveform data and extract the amplitude, and then compute the parameter values for the waveform, simulate the equation, and plot the data.

7. Conclusions

A brief description of the J-A model was presented with some additional alterations. The model was created in the MATLAB/Simulink workspace with the aid of well-known numeric solvers. Physical curves were measured, and an optimization process was developed using a random search method. The fitting process, cost function, and algorithm have been described. The biggest drawback of this model is that it is random in nature, so the optimization result can vary with repeated iterations with the same initial conditions. The larger the searching bounds used for the minimization search, the longer the computation time will become, but concurrently, a higher chance of finding the global minimum of the SSE value is to be expected. The fitting process has a strong local searching power but still enables global searching to some degree because the random numbers have a Gaussian probability distribution. Designing a more efficient algorithm and implementing an excitation dependence on the model parameters will be the subject of future research. A formula that describes the parameter values on the excitation field waveform amplitude has been introduced and shows a good fit with experimental data with a wide variety of excitations.

Acknowledgments

The authors thank for the financial support from the GRANT FEI 2022 project for the grant specified by the index FEI-2022-82, which helped in the research.

References

[1] P. Gębara, R. Godzur, K. Chwastek, *Acta Phys. Pol. A* **137**, 918 (2020).

[2] G. Bertotti, in: *Encyclopedia of Materials: Science and Technology*, Eds. K.H.J. Buschow, R.W. Cahn, M.C. Flemings, B. Ilschner, E.J. Kramer, S. Mahajan, P. Veyssière, Elsevier, 2001, p. 4798.

[3] C.D. Graham Jr., *J. Appl. Phys.* **53**, 8276 (1982).

[4] A. Ktena, D.I. Fotiadis, C.V. Massalas, in: *Advances in Scattering and Biomedical Engineering*, Eds. D.I. Fotiadis, C.V. Massalas, 2004, p. 313.

[5] C.S. Schneider, S.D. Gedney, N. Ojeda-Ayala, M.A. Travers, *Phys. B: Physics of Condens. Matter* **607**, 412802 (2021).

[6] P. Gębara, R. Gozdur, K. Chwastek, *Acta Phys. Pol. A* **134**, 1217 (2018).

[7] R.G. Harrison, *IEEE Trans. Magn.* **39**, 950 (2003).

[8] R. Gozdur, P. Gębara, K. Chwastek, *Open. Phys* **16**, 266 (2018).

[9] H. Hauser, *J. Appl. Phys.* **75**, 2584 (1994).

[10] D.C. Jiles, D.L. Atherton, *J. Magn. Magn. Mater.* **61**, 48 (1986).

[11] A. Benabou, J.V. Leite, S. Clénet, C. Simão, N. Sadowski, *J. Magn. Magn. Mater.* **320**, e1034 (2008).

[12] S.E. Zirka, Y.I. Moroz, R.G. Harrison, K. Chwastek, *J. Appl. Phys.* **112**, 043916 (2012).

[13] R. Du, P. Robertson, *IEEE Trans. Magn.* **51**, 1 (2014).

[14] A. Jakubas, K. Chwastek, *Materials* **13**, 170 (2020).

[15] COMSOL Multiphysics, *Modeling Hysteresis Effects*, 2008.

[16] A. Przybył, P. Gębara, R. Gozdur, K. Chwastek, *Energies* **15**, 7951 (2022).

[17] R. Gozdur, P. Gębara, K. Chwastek, *Energies* **13**, 1491 (2020).

[18] V. Khemani, M.H. Azarian, M.G. Pecht, *Energies* **3**, 364 (2022).

[19] R. Marion, R. Scorretti, N. Siauve, M. Raulet, L. Krähenbühl, *IEEE Trans. Magn.* **44**, 894 (2008).

[20] B. Bai, J. Wang, K. Zhu, in: *2011 Int. Conf. on Electrical Machines and Systems*, Beijing 2011.

[21] X. Wang, D.W.P. Thomas, M. Summer, J. Oauk, S.H.L. Cabral, *COMPEL Int. J. Comput. Math. Electric. Electron. Eng.* **28**, 493 (2009).

[22] K. Chwastek, J. Szczygłowski, *J. Magn. Magn. Mater.* **314**, 47 (2017).

[23] E.D.M. Hernandez, C.S. Muranaka, J.R. Cardoso, *Phys. B: Condens. Matter* **275**, 212 (2000).

[24] M.F. Jaafar, M.A. Jabri, in: *2013 Int. Conf. on Electrical Engineering and Software Applications*, 2013.

[25] M. Nowicki, *Materials* **2018**, 11 (2021).

[26] S. Steentjes, M. Petrun, G. Glehn, D. Dolinar, K. Hameyer, *Appl. Phys. Lett.* **95**, 172510 (2009).

[27] U. Rupnik, A. Alić, D. Miljavec, *Energies* **15**, 6760 (2022).

[28] D.C. Jiles, J.B. Thoelke, M.K. Devine, *IEEE Trans. Magn.* **28**, 27 (1992).

[29] E.D.M. Hernandez, C.S. Muranaka, J.R. Cardoso, *Phys. B: Condens. Matter* **275**, 212 (2000).

[30] R. Gozdur, P. Gębara, K. Chwastek, *Acta Phys. Pol. A* **136**, 689 (2019).

[31] Š. Gans, J. Molnár, in: Electrical Engineering and Informatics 13: Proc. of the Faculty of Electrical Engineering and Informatics of the Technical University of Košice, 2022.

[32] S. Grys, M. Najgebauer, *Measurement* **174**, 108962 (2021).

[33] P. Petrovic, N. Mitrovic, M. Stevanovic, P. Pejovic, "Hysteresis Model of Magnetic Materials Using the Jiles–Atherton Model".

[34] R.L. Iman, in: *Encyclopedia of Quantitative Risk Analysis and Assessment*, John Wiley & Sons, 2008.

[35] T.M. Le, B. Fatahi, H. Khabbaz, W. Sun, *Appl. Math. Modell.* **41**, 236 (2017).

[36] R.A. Naghizadeh, B. Vahidi, S.H. Hosseinian, *COMPEL Int. J. Comput. Math. Electric. Electron. Eng.* **31**, 1293 (2012).